

Structural features and stability of Spanish sepiolite as a potential catalyst

Aqeel Al-Ani ^{a *}; Ralf Gertisser^b and Vladimir Zholobenko^{a †}

^a *School of Chemical and Physical Sciences, Keele University, Keele, Staffordshire, ST5 5BG, United Kingdom*

^b *School of Geography, Geology and the Environment, Keele University, Keele, Staffordshire, ST5 5BG, United Kingdom*

Abstract

Sepiolite-based catalysts loaded with potassium hydroxide were prepared via the wet impregnation and ion-exchange methods and evaluated as catalysts in base-assisted reactions, such as transesterification of renewable oils. The structural features of these catalysts were characterised in detail by variable-temperature in situ X-ray diffraction, N₂ adsorption-desorption, scanning electron microscopy with energy-dispersive X-ray analysis and in situ FTIR spectroscopy. Although a high yield of fatty acid methyl esters was achieved in transesterification reactions in the presence of K-containing sepiolite, this system showed significant deactivation due to its structural degradation and loss of the active component during the reaction and regeneration cycles. This work demonstrates for the first time how the thermal and structural stability of sepiolite based systems can affect their performance, which is an essential issue that has not been sufficiently addressed in recent research related to the catalytic applications of these materials.

Keywords:

Structural stability, in situ XRD, Sepiolite, Transesterification, Microwave Catalysis

^{*, †} Corresponding authors:

Aqeel Al-Ani, e-mail address: a.a.t.al-ani@keele.ac.uk

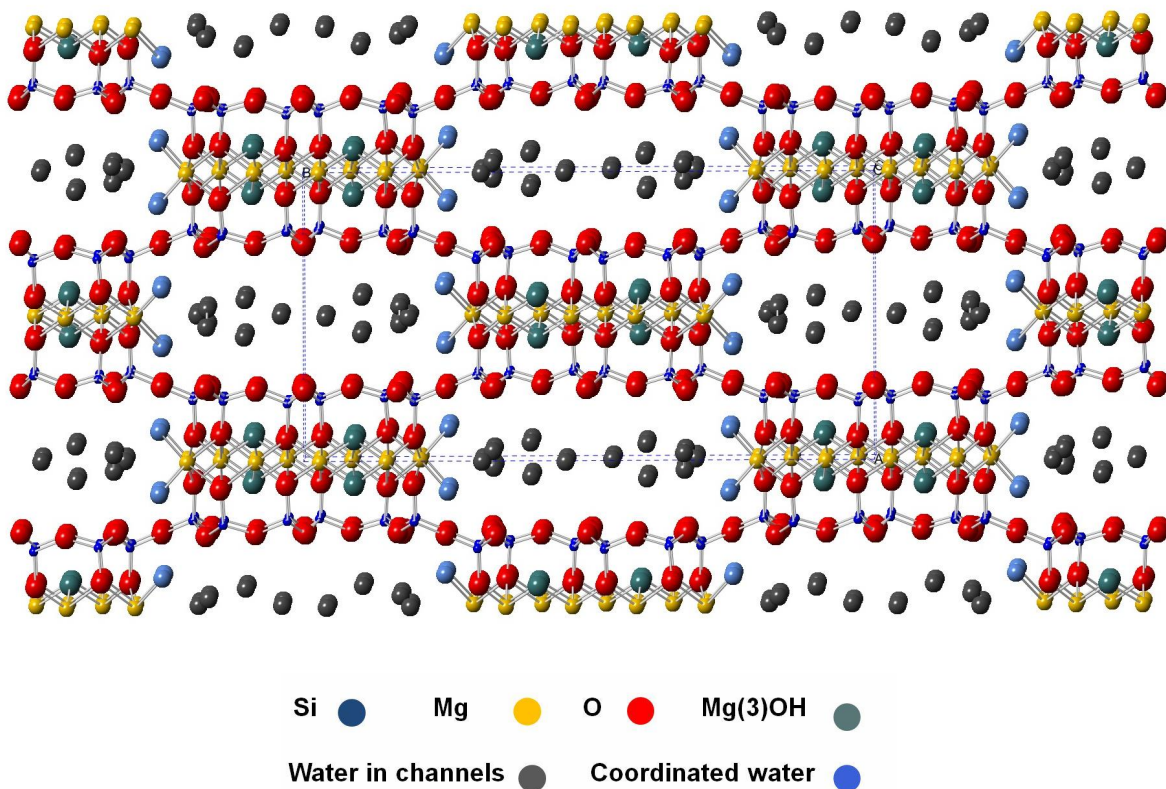
Vladimir Zholobenko, e-mail address: v.l.zholobenko@keele.ac.uk

29 **1. Introduction**

30 Nanoporous materials have been used in a host of catalytic applications owing to their versatile pore
31 networks, enhanced reactivity, stability, chemical functionality and high surface area (Corma et al.,
32 2006; Somorjai and Na, 2015; Mota et al., 2016). Many studies have illustrated the use of alkaline,
33 alkaline earth and transition metal oxides supported on nanoporous materials with the pore size of
34 ~1-100 nm, such as silicas, clays and zeolites prepared by impregnation, ion exchange and
35 precipitation as highly active catalysts (Corma and Martin-Aranda, 1991; Gedanken et al., 2016).
36 One of the processes for the production of an environmentally friendly fuel from vegetable oils and
37 animal fats is the transesterification reaction between triglycerides (TGs) in oils or fats and an
38 alcohol, which is carried out in the presence of an acid or base catalyst yielding fatty acid methyl
39 esters (FAMEs) and glycerol. For this reaction, heterogeneous catalysis can offer a greener route
40 with potential advantages including the elimination of the quenching step, separation of the products
41 and associated aqueous waste (Gandía et al., 2018).

42 Sepiolite (Sep), often in close association and intergrowth with palygorskite, is known from many
43 localities worldwide but is typically found in only small amount compared to other minerals that
44 form under similar geological conditions. The low specific gravity, high porosity and capacity to
45 float on water led to the original name *öMeerschaumö* (German for *öfoam of the seaö*) by Abraham
46 Gottlob Werner. Later, based on its similarity with cuttlebone, the internal shell of cuttlefish, the
47 name *ösepioliteö* from Greek *ösepiönö* (cuttlebone) and *ölithosö* (stone) was given to the mineral for
48 a find in the Piedmont region of Italy. Sep requires alkaline conditions, with high activities of silicon
49 and magnesium (Singer, 1989), and is also often associated with low latitudes and arid to semi-arid
50 climates. Environments of formation include marine, lacustrine and lagoonal continental sediments,
51 soils, palaeosols and calcretes (Deer et al., 1992). Replacement of pre-existing minerals such as
52 magnesite (Yeniyol, 1986), hydrothermal alteration (e.g. Ehlmann et al., 1962; Irkeç and Ünlü,
53 1993) and a role of biomineralisation (e.g. Leguey et al., 2010) have also been suggested for the
54 formation of Sep. Large, economically valuable Sep deposits originate mostly from formation in
55 shallow seas and lakes as chemical sediments. At Eski ehir (Turkey), the richest Sep mining field in
56 the world, Sep occurs as layers and nodules in Neogene lacustrine sediments (Kadir et al., 2016).
57 Other notable Sep occurrences are in the United States, the Czech Republic, Greece, France and
58 Spain. The latter includes Sep-rich deposits in southern and central Spain associated with lagoonal
59 and lacustrine environments (e.g. Galán and Ferrero, 1982; Galán and Castillo, 1984; Torres-Ruíz et
60 al., 1994; Armenteros et al., 1995; Bustillo and Alonso-Zarza, 2007).

61 Together with palygorskite, Sep is a member of the palygorskite group of clay minerals, which
 62 belong to the sheet silicate (phyllosilicate) group of the silicates (Deer et al., 1992). These minerals
 63 are characterised by the same basic building blocks, namely a tetrahedral sheet and one of two kinds
 64 of octahedral sheets, combined to form composite mineral structures. In contrast to other sheet
 65 silicates, Sep, a fibrous hydrated magnesium silicate with the ideal chemical formula
 66 $Mg_4Si_6O_{15}(OH)_2 \cdot 6H_2O$ (the formula $Mg_8Si_{12}O_{30}(OH)_4 \cdot 4(H_2O) \cdot nH_2O$ is also used in the literature),
 67 lacks continuous octahedral sheets (Figure 1). The tetrahedral sheets are continuous; however,
 68 ribbons rather than sheets of octahedra leave channels (0.36×1.06 nm in size) in the Sep structure
 69 that can accommodate water and organic molecules (Deer et al., 1992). Furthermore, Sep is
 70 characterised by a high specific surface area and good surface affinity towards organic and inorganic
 71 species (Kadir and Akbulut, 2003; Sabah and Çelik, 2005; Suarez et al., 2016).



73
 74 **Fig. 1.** Sepiolite structure (the blue dotted line indicates the unit cell size).

75 There has been a great deal of interest in utilising the sorptive, rheological and catalytic properties of
 76 Sep in many industrial applications (Alvarez, 1984). For instance, Sep has been recently used as
 77 catalyst support for green chemistry applications (Figen et al., 2018). Furthermore, a number of
 78 studies have been focused on the applications of natural clay minerals including Sep, red mud and
 79 bentonite as catalysts for the production of renewable fuels. Alves et al. (2014) utilised treated

80 smectite clay with potassium fluoride in transesterification of soybean oil utilising the clay as a solid
81 catalyst. Soetaredjo et al. (2011) examined the performance of potassium hydroxide impregnated
82 bentonite as a catalyst for palm oil conversion. Agustain et al. (2012) used three metal (Ba, K and
83 Na) hydroxides supported on bentonite as catalysts for methanolysis of jatropha curcas oil.
84 Degirmenbasi et al. (2014) used K_2CO_3 loaded Sep as a solid catalyst in transesterification of canola
85 oil. Xu et al. (2013) employed red mud containing strongly basic active sites on the surface as a
86 catalyst for biodiesel production from soybean oil. Most authors reported a high yield of FAMEs,
87 typically over 90%, after several hours of the reaction time at temperatures above 65°C.

88 Important problems for heterogeneous systems, which can affect the catalytic performance, are
89 structural integrity, thermal stability and the loss of active phases from the catalyst. A considerable
90 challenge in an industrial application is maintaining the high catalyst activity for a number of
91 reaction and regeneration cycles. However, many published reports do not describe the structural
92 characterisation of the clay based catalysts before and after the reaction studies, which are often
93 limited to a very small number, if any, of the successive runs on regenerated catalysts.

94 In this paper, potassium hydroxide loaded Spanish Sep has been prepared via wet impregnation and
95 ion-exchange, and then used for the production of biofuel from both non-edible and edible oils using
96 microwave heating. The aim of the present study is twofold: to carry out a detailed structural
97 characterisation of the Sep-based catalyst both before and after the reaction and to evaluate the
98 structure - performance relationship in the transesterification reaction for the production of biofuel
99 from renewable feedstock for sustainable and clean energy applications.

100 **2. Experimental**

101 The Spanish Sep (ACS reagent) was obtained from Sigma-Aldrich. Potassium hydroxide (86%),
102 methanol, sodium hydroxide (99%) and n-heptane (analytical grade, >99.99%) were purchased from
103 Fisher Scientific. The grapeseed oil was supplied by Now Solutions (USA), refined rapeseed oil was
104 purchased from a local market and castor oil was obtained from Fisher Scientific. Methyl
105 heptadecanoate (analytical GC standard, >99.99%) was supplied by Sigma-Aldrich.

106 Two types of catalysts were prepared by impregnation (K-Sep-Imp) and ion-exchange (K-Sep-IE)
107 procedures. These were characterised before and after the reaction using in situ variable-temperature
108 X-ray diffraction (VT XRD), scanning electronic microscopy with energy-dispersive X-ray analysis
109 (SEM-EDX), thermogravimetric analysis (TGA), nitrogen adsorption-desorption and in situ FTIR
110 spectroscopy. Detailed procedures are provided in the Electronic Supplementary Material (ESM).

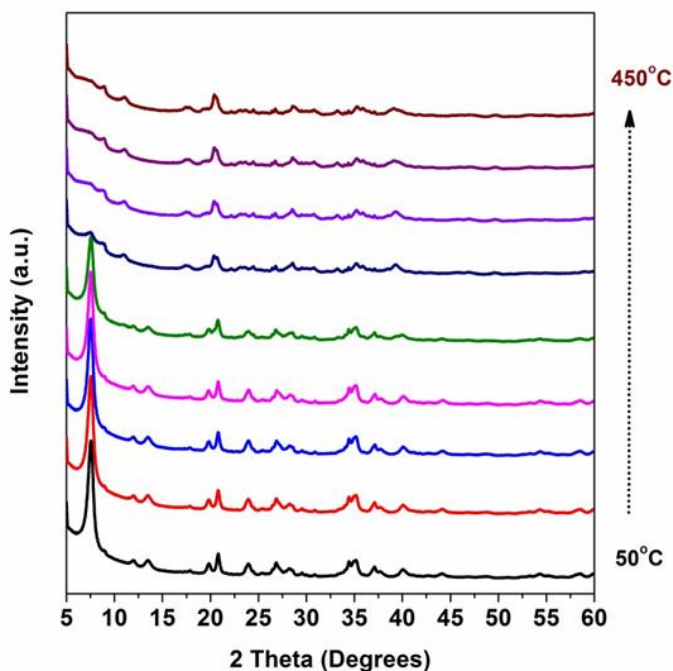
111 Following the transesterification reaction (Figure S1), the catalysts were separated, rinsed with
112 methanol, dried at 60°C and reactivated under the same conditions as prior to the initial reaction and
113 utilised again. The same reaction conditions were used in four consecutive runs for the recycled
114 catalysts.

115 **3. Results and discussion**

116 One of the most important characteristics of a working catalyst is its structural stability. This can be
117 affected at different stages of the catalyst activation and regeneration or in the course of the reaction
118 itself. The structural properties of the Sep-based catalysts were monitored by both in situ and ex situ
119 XRD, FTIR and N₂ adsorption. Figures 2 and S2 (ESM) present the VT-XRD patterns of the Sep
120 and K-Sep-Imp recorded at different calcination temperatures. There are clear changes in the
121 patterns of both materials recorded above 200°C. For Sep in particular, the intensity of the 110
122 reflection at 7.48° (1.18 nm d-value; a summary of the indexed XRD reflections is given in Table
123 S2), which corresponds to the interlayer distance in the clay structure, decreased significantly,
124 becoming negligible above 300°C. Similar intensity changes were observed for the same reflection
125 (1.19 nm d-value) in the patterns of the K-Sep-Imp sample. It is suggested that the layered structure
126 of the catalyst collapsed during the high temperature calcination. The observed structural changes
127 are not reversible as the VT-XRD patterns, recorded for both materials upon cooling, did not change.
128 Our data are in accord with the findings of Preisinger (1959), Dany and Nadiye-Tabbiruka (1975)
129 and Grillet et al. (1988) indicating that the Sep structure showed significant changes upon heating
130 above 150°C, which was accompanied by the loss of water and microporosity. In addition, an in situ
131 variable-temperature synchrotron investigation (Post et al., 2007) and a number of ex situ studies
132 (Kok, 2013; Pi kin, 2013; Yenyol et al., 2014) on Sep samples calcined up to 900°C demonstrated
133 the folding of the Sep structure resulting from its dehydration above 320°C with the loss of the
134 micropore channels, which was followed by the formation of two "anhydrous" Sep phases at ~460
135 and 650°C. These results and most literature data, however, disagree with those presented by
136 Degirmenbasi et al. (2014), who suggested that heating Sep to 500°C did not cause any change in the
137 catalyst structure. Our nitrogen adsorption and TGA-DSC data support the VT-XRD finding. Indeed,
138 the BET surface area (S_{BET}) of Sep decreased with increasing activation temperature from 325 to 130
139 m²/g (Figures 3, 4 and S3, ESM); the BET surface area of K-Sep-Imp was below 100 m²/g.
140 Therefore nitrogen adsorption and XRD data clearly demonstrate that potassium introduction and
141 activation at elevated temperatures lead to considerable structural degradation and a significant
142 decrease in the S_{BET} . In addition, the micropores present in the original Sep (~0.8 nm in diameter) in
143 the spaces between the silicate layers were no longer detected for the samples activated at
144 temperatures above 200°C. These results are also supported by previous research (Gómez-Avilés et

145 al., 2013; Pi kin et al., 2013; Pozo et al., 2014; Suarez et al., 2016). While these publications did
146 confirm the high surface area of Sep and indicate the presence of micropores, to the best of our
147 knowledge, our work is the first to present a detailed characterisation of a series of thermally treated
148 Sep samples in the region of low P/P_0 values corresponding to the micropore filling by nitrogen.

(a)



(b)

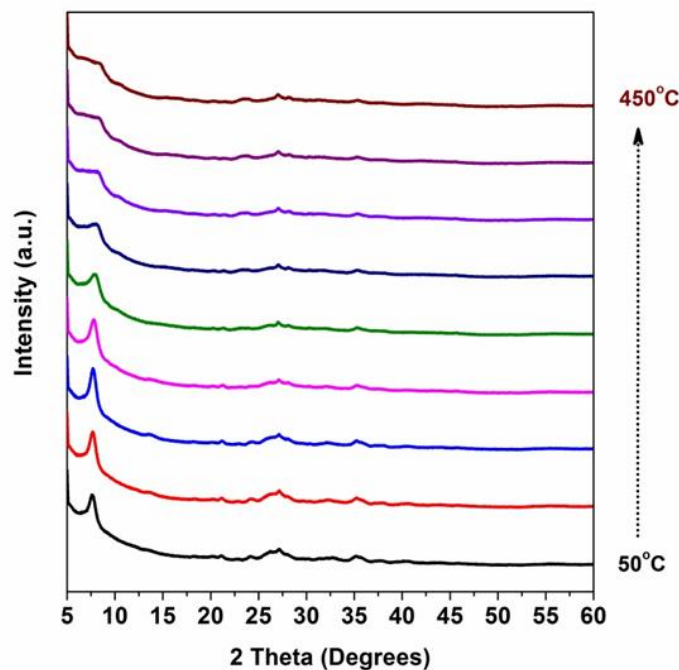
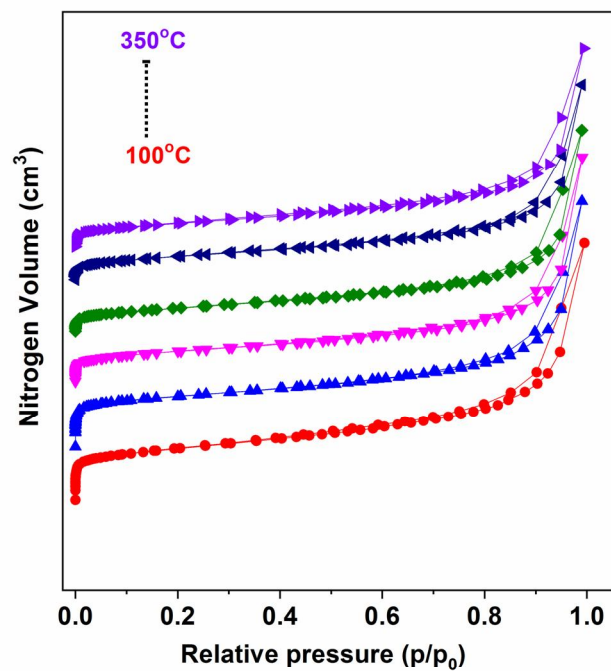


Fig. 2. In situ VT XRD patterns collected every 50°C (heating up) of (a) parent Sep catalyst and (b) K-Sep-Imp. Patterns are offset for clarity.

(a)



(b)

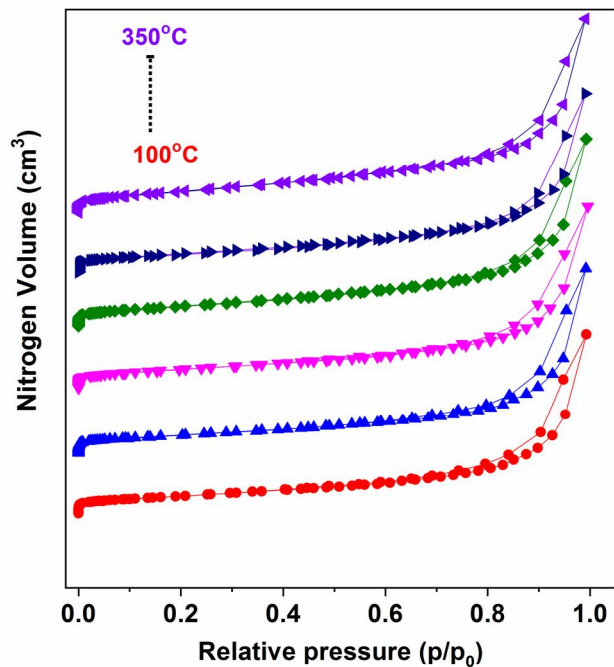
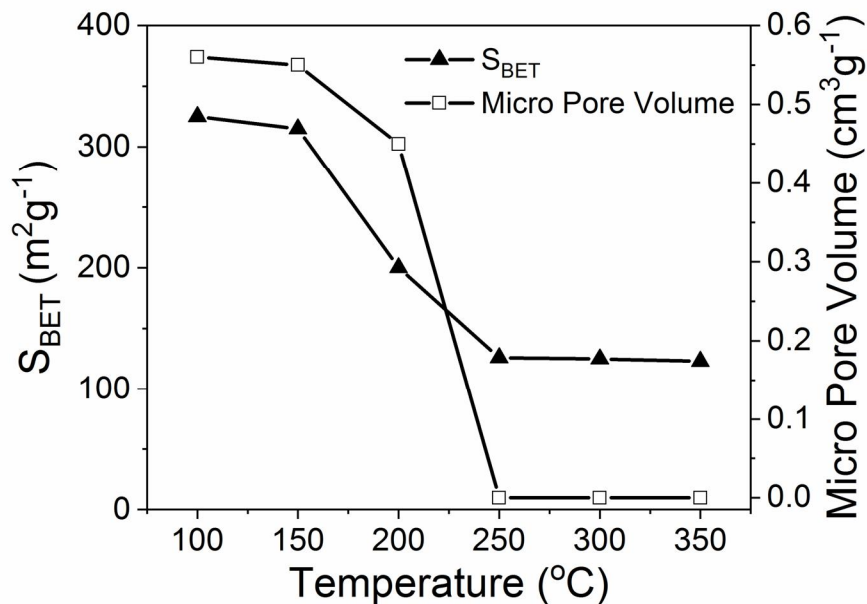


Fig. 3. Nitrogen adsorption isotherms for (a) Sep and (b) K-Sep-Imp activated at 100-350°C in 50°C steps. Isotherm traces are offset for clarity.

(a)



(b)

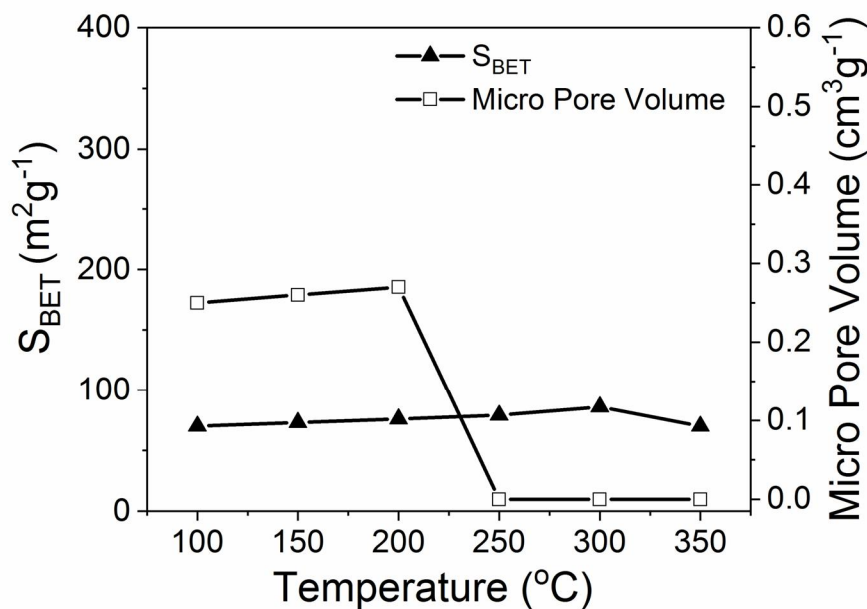
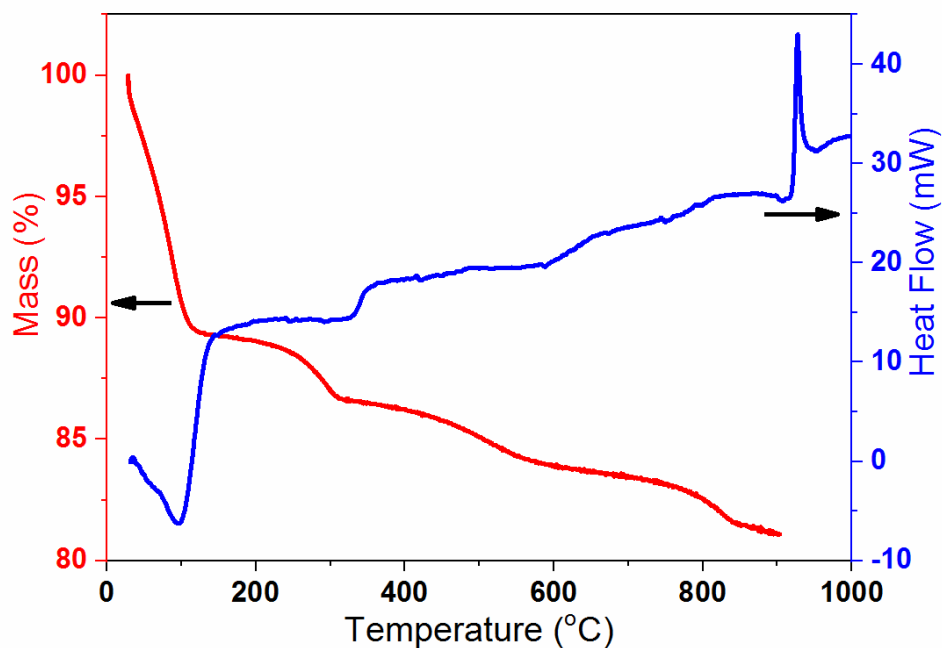


Fig. 4. Specific surface area and micropore volume data as a function of the activation temperature for (a) Sep and (b) K-Sep-Imp.

151 Although the thermal treatment process is essential for the decomposition of the metal precursor,
152 there is a significant change in the catalyst properties caused by heating above 250°C, which is
153 associated with the loss of water and the collapse of the layered structure. In agreement with
154 previous studies (Hayashi et al., 1969; Kok, 2013; Ogorodova et al., 2016), our TGA-DSC data
155 confirmed the stepwise removal of water from Sep, which accounts for ~9% of the mass loss at
156 100°C and ~4% at 250-300°C (both steps are endothermic processes as expected) with the total mass

157 loss of ~18% by 900°C (Figure 5). The exothermic peak observed at 850°C corresponds to a high
158 temperature phase transition resulting in a complete loss of the Sep structure. The data obtained for
159 K-Sep were largely similar, ~15% of the mass loss at 400°C and ~18% by 900°C, but showing a
160 more gradual removal of water from this material as compared to the parent Sep sample (Hayashi et
161 al.,1969).

(a)



(b)

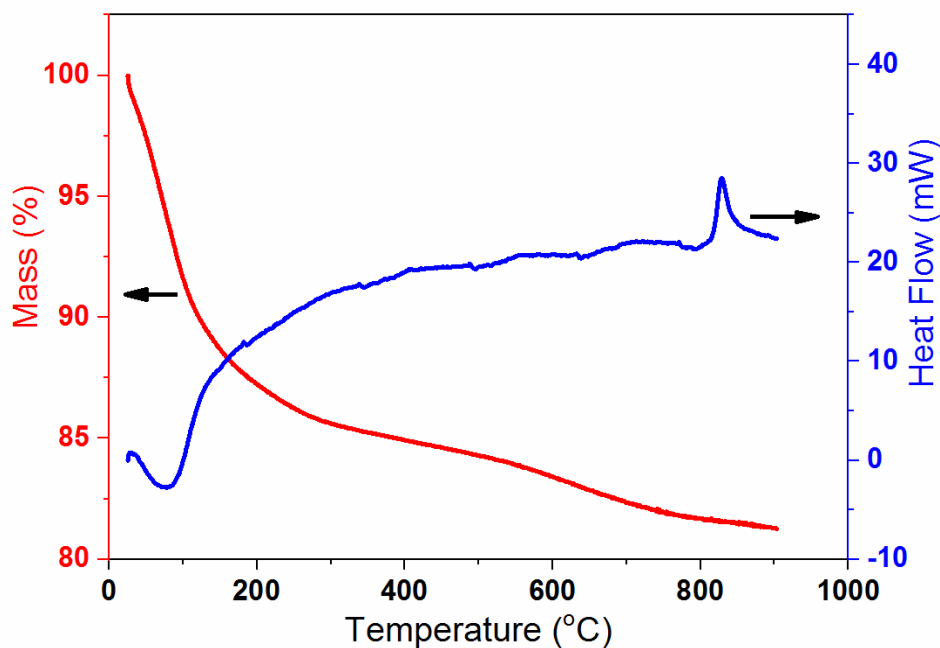


Fig. 5. Thermogravimetric analysis data for (a) Sep and (b) K-Sep.

162 Chemical analysis data and SEM images for Sep, K-Sep-Imp and used K-Sep-Imp are presented in
 163 Table 1 and Figure 6, respectively. The chemical analysis results correspond to the empirical
 164 formula $2\text{MgO} \cdot 3\text{SiO}_2 \cdot n\text{H}_2\text{O}$ of the original sample. The potassium content of 6.1 wt% in K-Sep
 165 indicates ~60% efficiency of the impregnation procedure. The potassium concentration decreased
 166 significantly after the reaction-regeneration cycle, whereas there were no changes to the morphology
 167 of K-Sep-Imp and used K-Sep-Imp, which would have implications for the catalytic performance of
 168 these materials. Table 1 also summarises the S_{BET} values obtained for the studied Sep based catalysts
 169 Interestingly, the nitrogen adsorption data show that the specific surface area of used K-Sep catalysts
 170 did not change noticeably after the reaction-regeneration cycle being in the region of $\sim 80 \text{ m}^2/\text{g}$, but
 171 the micropore volume decreased significantly, which is probably due to the micropore blockage by
 172 the reacting species that could not be removed under the relatively mild regeneration conditions. A
 173 greater reduction in the S_{BET} may be expected due to the loss of micropores in the used catalysts,
 174 however, this is probably compensated by the removal of the K-containing species from the external
 175 surface (see below).

176

177 **Table 1.** Elemental analysis and nitrogen adsorption data for Sep based catalysts.

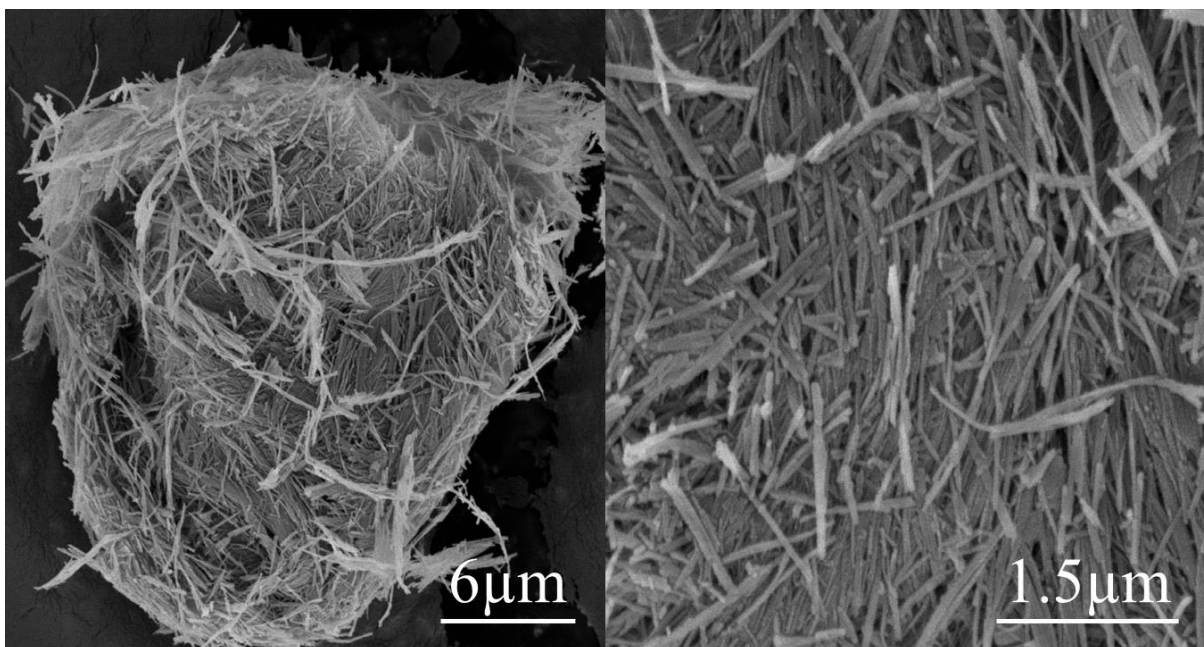
<i>Material</i>	<i>Elemental composition</i>				S_{BET} (m^2/g) ^a	V_{micro} (cm^3/g) ^a
	<i>Silicon</i>	<i>Magnesium</i>	<i>Potassium</i>	<i>Sodium</i>		
<i>Parent Sep</i>	22.5	13.3	<0.2	-	195	0.39
<i>K-Sep-Imp</i>	17.3	13.4	6.1	-	75	0.27
<i>K-Sep-Imp used</i>	17.2	13.3	3.2	-	70	0.01
<i>K-Sep-IE</i>	19.7	11.8	4.0	4.6	85	0.28
<i>K-Sep-IE used</i>	19.8	12.0	2.5	1.8	80	0.01

178

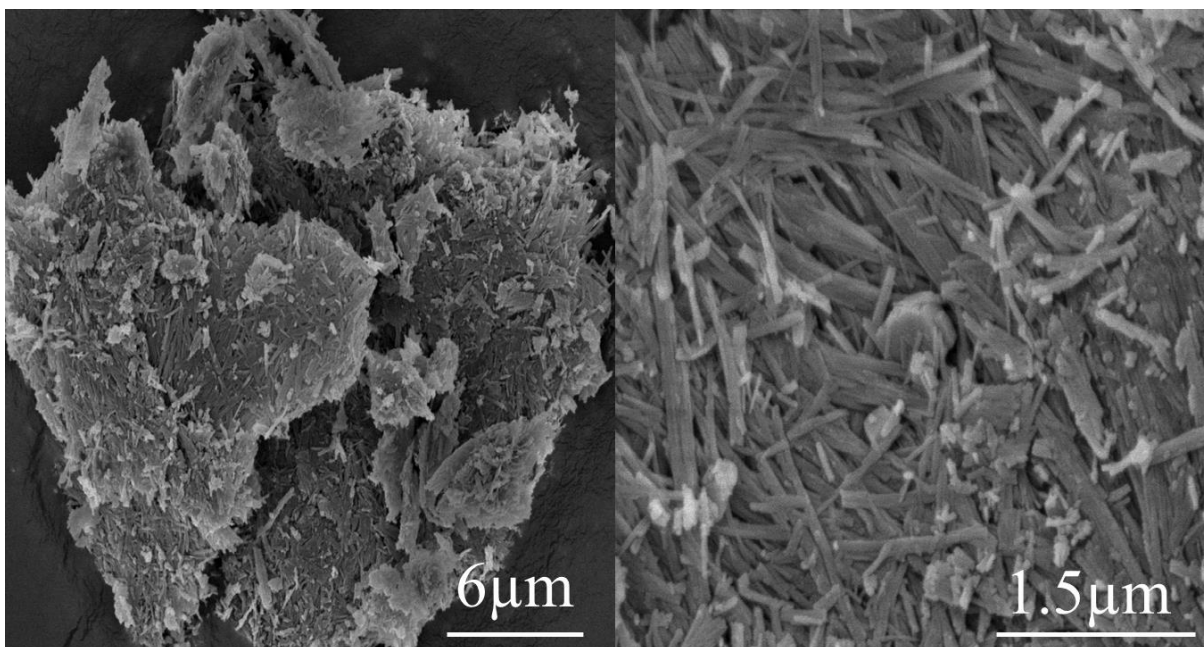
179 ^a All materials were activated at 200°C.

180

(a)



(b)



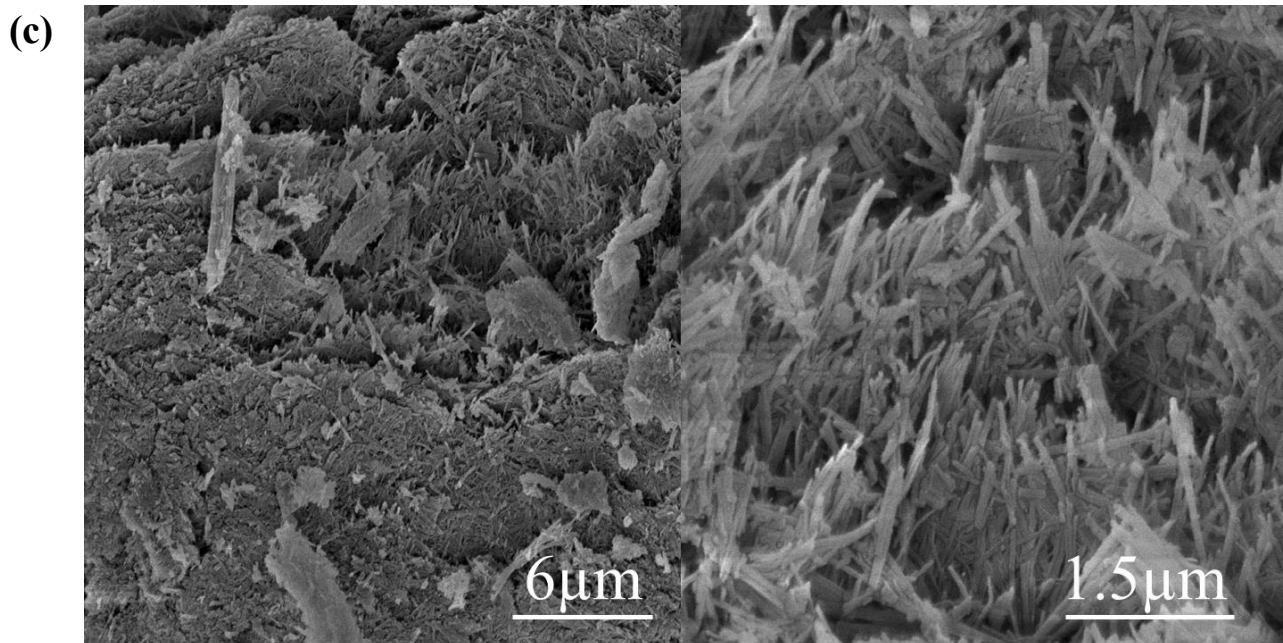


Fig. 6. SEM images of (a) Sep, (b) K-Sep-Imp and (c) K-Sep-Imp following reaction and regeneration.

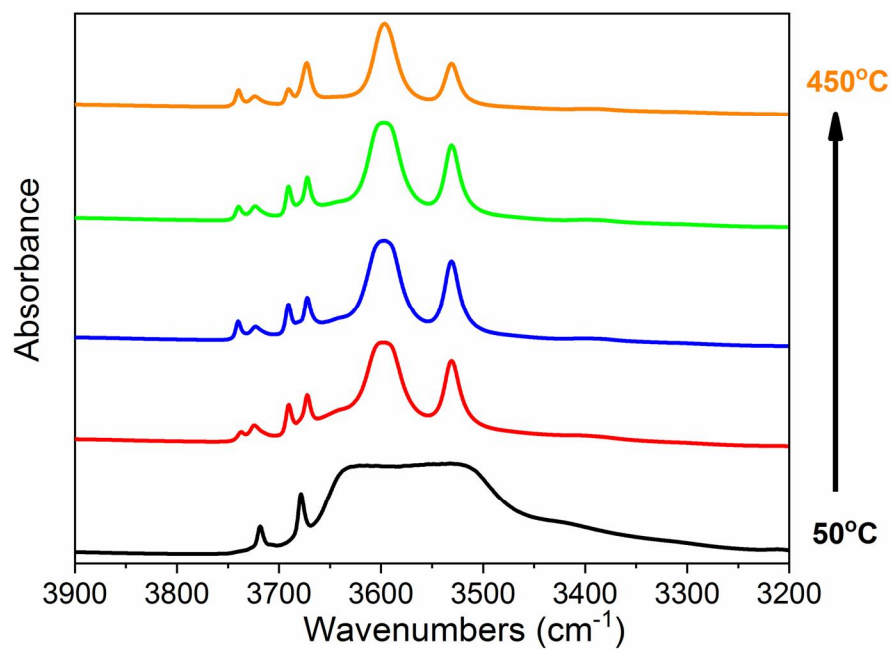
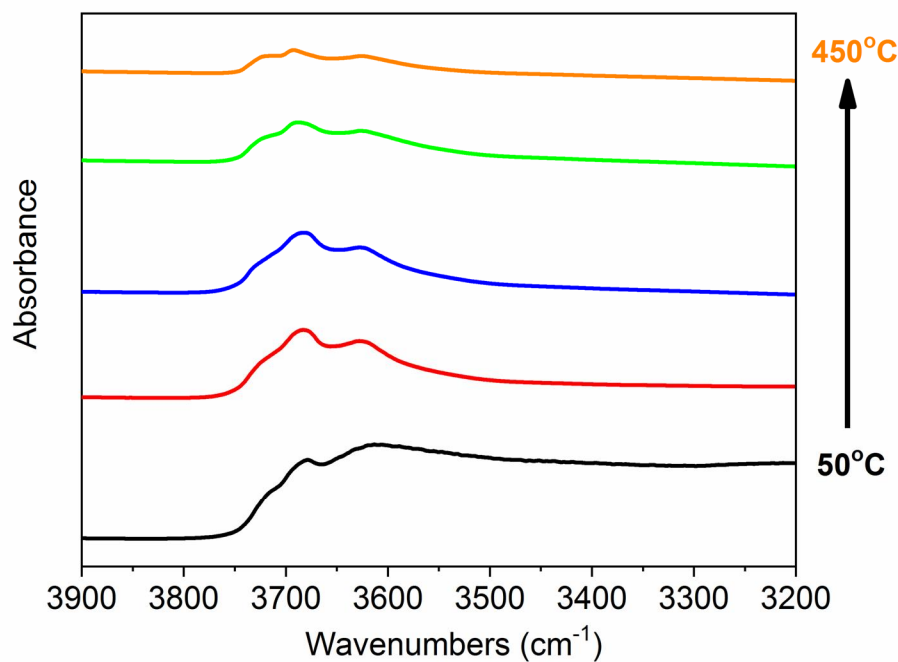
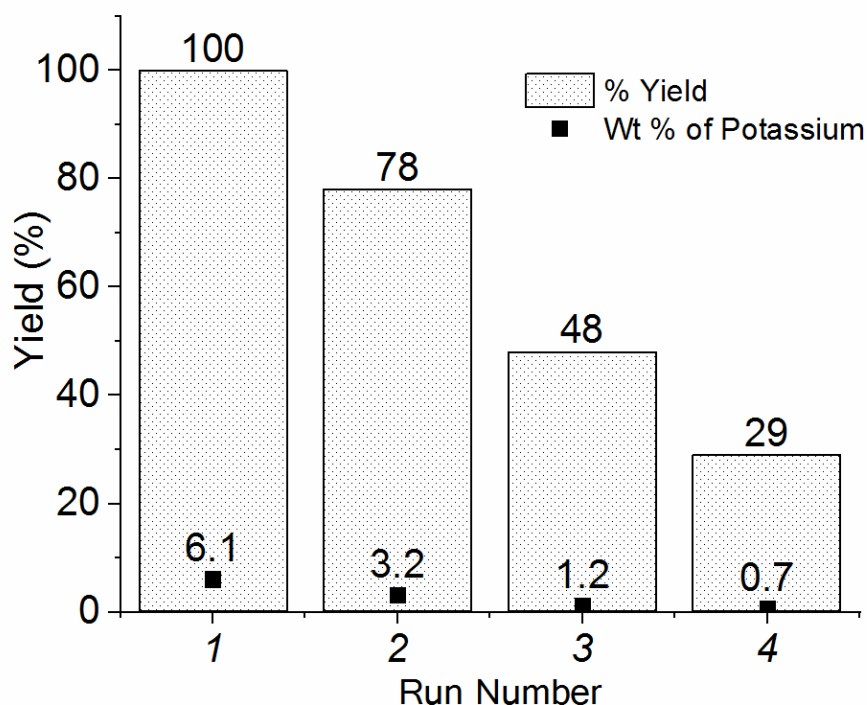
(a)**(b)**

Fig. 7. The OH-region of FTIR spectra for (a) Sep and (b) K-Sep-Imp catalysts activated at 50-450°C in 100°C steps. Spectra are offset for clarity.

185 The OH region of the FTIR spectra for Sep and K-Sep-Imp are presented in Figure 7 (the wide range
186 spectra, from 1000 to 6000 cm^{-1} including the overtones and combination frequencies, are available
187 in ESM, Figure S4). The evolution of the spectral bands of different types of OH groups was
188 followed in situ during sample dehydration between 30 and 450°C. The initial spectra were
189 dominated by the broad feature at $\sim 3650\text{-}3300\text{ cm}^{-1}$ owing to weakly bound water molecules, which
190 are commonly referred to as "zeolitic water" in the mineralogical literature, and which were removed
191 upon mild dehydration at 150°C. Two overlapping bands at 1625 and 1616 cm^{-1} were also observed
192 in the region of OH-bending vibrations. The spectra of the dehydrated samples exhibited six peaks in
193 the region of stretching O-H vibrations. In agreement with the literature (Hayashi et al., 1969; Frost
194 et al., 2001; Ruiz et al., 2010; Giustetto et al., 2010; Bukas et al., 2013; Post et al., 2014; Chryssikos
195 et al., 2015), the peaks at 3740 and 3724 cm^{-1} are assigned to Si-OH groups of the tetrahedral silicate
196 layer and those at 3691 and 3673 cm^{-1} to Mg(3)-OH groups in the octahedral sheets of the Sep
197 structure. The bands at 3597 and 3531 cm^{-1} are attributed to water molecules coordinated to Mg
198 cations, which is supported by the presence of a single band at 1616 cm^{-1} in the region of bending
199 OH vibrations. Interestingly, these peaks persisted in the spectra of the samples dehydrated in
200 vacuum at 450°C for 5 hours. It should be noted that there are minor variations in the position of the
201 absorption bands reported in the literature, which is probably related to the fact that most of the
202 previous data were obtained using ex situ experiments on calcined samples or KBr disks with
203 somewhat uncertain degree of control over the hydration and dehydration processes. Although the
204 interpretation of the spectra has been supported by extensive NIR characterisation of Sep (Frost et
205 al., 2001; Ruiz et al., 2010; Giustetto et al., 2010; Chryssikos et al., 2015), a different assignment
206 could not be completely ruled out. For instance, two OH bands at 3734 and 3583 cm^{-1} were observed
207 in the spectra of magnesium oxide calcined at 500°C (Hadjiivanov, 2014). The spectra of K-Sep
208 dehydrated at elevated temperatures displayed rather broad overlapping bands between 3750 and
209 3600 cm^{-1} . This is in agreement with our VT-XRD and nitrogen adsorption data indicating
210 considerable structural degradation upon KOH impregnation and calcination of this material.

211 The structural stability, high surface area and strong bonding with the active phase preventing the
212 loss of the active sites are essential characteristics of a supported catalyst (Romero et al, 2016).
213 Figure 8 presents a comparison of the catalytic performance of K-Sep-Imp in transesterification of
214 triglycerides over several reactions ó regeneration cycles. These data demonstrate a significant
215 deactivation of K-Sep-Imp, which can be linked to its structural integrity and loss of the active sites.
216 Although we obtained high yield and selectivity of FAMES in the presence of K-Sep-Imp and K-
217 Sep-IE, these materials lack long-term stability in the methanolysis reaction. A considerable change

218 in the catalyst structure was found after calcination at elevated temperatures, accompanied by the
219 loss of water and a significant reduction in its surface area. In contrast to our results and the data
220 available in the literature, Degirmenbasi et al. (2014) concluded that a higher catalytic activity of
221 Sep impregnated with K_2CO_3 in the transesterification of canola oil is achieved following its
222 calcination to $500^\circ C$, apparently resulting in a catalyst more resistant toward the leaching of the
223 active phase. However, our structural characterisation, chemical analysis and catalytic data for the
224 Sep-based catalysts that were calcined or regenerated at temperatures between 250 and $450^\circ C$
225 provide no evidence of enhanced catalytic performance or improved structural stability following the
226 high temperature treatment. In addition, characterisation of the regenerated catalysts demonstrated
227 that the K^+ ions were leaching out during the transesterification reaction or the regeneration step,
228 which was accompanied with a significant drop in the yield of FAMES in the subsequent catalytic
229 run from 100% to 78% . A similar drop in activity was observed for the K-Sep-IE.



230

231 **Fig. 8.** Catalytic performance of the fresh and used K-Sep-Imp in the transesterification of grapeseed
232 oil at $160^\circ C$ and the wt% of potassium in these catalysts.

233 Furthermore, in a blank reaction run with $0.0035g$ of KOH (approximately the amount of potassium
234 hydroxide lost by K-Sep-Imp in the first reaction cycle), a triglyceride conversion of $\sim 75\%$ was
235 observed, confirming that potassium hydroxide in solution was active in the transesterification
236 reaction. Clearly, such effects should be taken into account, considering a significant number of

237 studies utilising clay-based catalysts either impregnated or ion-exchanged with potassium containing
238 compounds (Corma and Martin-Aranda, 1991; Villamiel et al., 2002; Ilgen and Akin, 2012;
239 Degirmenbasi et al., 2013, 2014; Chryssikos et al., 2015; Wang et al., 2017).

240

241 **4. Conclusion**

242 The application of heterogeneous catalysts in the production of biodiesel offers potential advantages
243 including lower cost, high stability and the ease of separation. In this work, Sep modified with K-
244 bearing compounds was prepared using impregnation and ion exchange procedures. The evolution of
245 the structural features of these catalysts was characterised in detail both before and after the reaction
246 by variable-temperature in situ XRD, N₂ adsorption-desorption, SEM-EDX and in situ FTIR
247 spectroscopy in order to evaluate their structure - performance relationship in the methanolysis of
248 vegetable oils. Our data demonstrated that the Sep structure undergoes irreversible changes upon
249 heating above 250°C, which are accompanied by the loss of water and OH groups. High-temperature
250 calcination resulted in dehydration of Sep followed by the folding of its structure with the loss of the
251 micropore channels and significant decrease in the surface area. Sep impregnation with KOH also
252 led to partial structural degradation and decrease in the surface area. Subsequent thermal treatment,
253 required for the decomposition of the metal precursor with the formation of an oxide on the Sep
254 support, can cause further structural changes associated with dehydration and the collapse of the
255 layered structure. Although high yield of FAMEs was obtained in transesterification in the presence
256 of K-Sep, our work demonstrated that both impregnated and ion-exchanged K-Sep lack long-term
257 stability in this reaction due to the loss of the active component during the recycling stages. Overall,
258 our reaction studies and extensive structural analysis point to a potentially significant contribution of
259 the homogeneously catalysed transformation of triglycerides in the presence of clay-based catalysts.

260

261 *Acknowledgments*

262 This work was supported by Ministry of Oil /Oil Marketing Company (SOMO), Baghdad, Iraq under
263 grant SL-144-01B. The authors appreciate the support of the Lennard-Jones Laboratories and the
264 School of Geography, Geology and the Environment at Keele University, UK, where this study was
265 carried out. We thank Karen Walker of Keele University for her help with obtaining SEM images.

266 **References**

- 267 Agustian, E., Ghozali, M., Savitri, R., Wuryaningsih, S., 2012. Biodiesel production of jatropha
268 curcas oil by bentonite as catalyst, Proceeding of International Conference on Sustainable Energy
269 Engineering and Application, 35-39.
- 270 Alvarez, A., 1984. Sepiolite: properties and uses. *Developments in Sedimentology*. 37, 253-287.
- 271 Alves, H.J., da Rocha, A.M., Monteiro, M.R., Moretti, C., Cabrelon, M.D., Schwengber, C.A.,
272 Milinsk, M.C., 2014. Treatment of clay with KF: New solid catalyst for biodiesel production. *Appl.*
273 *Clay Sci.* 91, 98-104.
- 274 Armenteros, I, Bustillo M.A.A., Blanco J.A. 1995. Pedogenic and groundwater processes in a closed
275 Miocene basin (northern Spain). *Sed. Geol.* 99, 17-36.
- 276 Bukas, V.J., Tsampodimou, M., Gionis, V., Chryssikos, G.D., 2013. Synchronous ATR infrared and
277 NIR-spectroscopy investigation of sepiolite upon drying. *Vib. Spect.* 68, 51-60.
- 278 Bustillo, M.A., Alonso-Zarza, A.M., 2007. Overlapping of pedogenesis and meteoric diagenesis in
279 distal alluvial and shallow lacustrine deposits in the Madrid Miocene Basin, Spain. *Sed. Geol.* 198,
280 255-271.
- 281 Chryssikos, G.D., Tsampodimou, M., Bukas, V., Stathopoulou, E.T., Gionis, V., 2015. Near-infrared
282 investigation of folding sepiolite. *Am. Miner.* 100(1), 195-202.
- 283 Corma, A., Martin-Aranda, R.M., 1991. Alkaline-substituted sepiolites as a new type of strong base
284 catalyst. *J. Cata.* 130(1), 130-137.
- 285 Corma, A., Huber, G.W., Iborra, S., 2006. Synthesis of transportation fuels from biomass: chemistry,
286 catalysts, and engineering. *Chem. Rev.* 106 (9), 4044-4098.
- 287 Dandy, A., Nadiye-Tabbiruka, M., 1975, The effect of heating in vacuo on the microporosity of
288 sepiolite. *Clays Clay Miner.* 23, 428-430.
- 289 Deer, W.A., Howie, R.A., Zussman, J., 1992. *An Introduction to the Rock-Forming Minerals.*
290 Prentice Hall (2nd edition); pp. 712.
- 291 Degirmenbasi, N., Boz, N., Kalyon, D.M., 2013. Transesterification of canola oil to biodiesel using
292 calcium bentonite functionalized with K compounds. *Appl. Catal. B: Envir.* 138, 236-242.
- 293 Degirmenbasi, N., Boz, N., Kalyon, D.M., 2014. Biofuel production via transesterification using
294 sepiolite-supported alkaline catalysts. *Appl. Catal. B: Envir.* 150, 147-156.
- 295 Ehlmann, A.J., Sand, L.B., Regis, A.J., 1962. Occurrences of sepiolite in Utah and Nevada. *Econ.*
296 *Geol.* 57, 1085-1094.
- 297 Figen, A.K., Me e, E., Filiz, B.C., Pi kin, S., 2018. Cobalt-boron loaded thermal activated Turkish
298 sepiolite composites (Co-B@ tSe) as a catalyst for hydrogen delivery. *Appl. Clay Sci.* 153, 95-106.
- 299 Frost, R.L., Locos O.B., Ruan, H., Klopogge, J.T., 2001. Near-infrared and mid-infrared
300 spectroscopic study of sepiolites and palygorskites. *Vib. Spect.* 27 (1), 1-13.

- 301 Galán, E., Castillo, A., 1984. Sepiolite-palygorskite in Spanish Tertiary basins: genetical patterns in
302 continental environments. *Developments in Sedimentology* 37, 87-124.
- 303 Galán, E., Ferrero, A., 1982. Palygorskite-sepiolite clays of Lebrija, Southern Spain. *Clays and Clay*
304 *Minerals* 30, 191-199.
- 305 Gandía, L.M., Navajas, A., Campo, I., Moral, A., Echave, J., Sanz, O., Montes, M., Odriozola, J.A.,
306 Arzamendi, G., 2018. Outstanding performance of rehydrated Mg-Al hydrotalcites as heterogeneous
307 methanolysis catalysts for the synthesis of biodiesel. *Fuel*. 211, 173-181.
- 308 Gedanken, A., Tangy, A., Pulidindi, I.N., 2016. SiO₂ beads decorated with SrO nanoparticles for
309 biodiesel production from waste cooking oil using microwave irradiation. *Energy & Fuels* 30(4),
310 3151-3160.
- 311 Giustetto, P., Seenivasan, K., Bordiga, S., 2010. Spectroscopic characterization of a sepiolite-based
312 Maya Blue pigment. *Periodicodi Mineralogia*. 21-37.
- 313 Gómez-Avilés, A., Aranda, P., Fernandes, F.M., Belver, C., Ruiz-Hitzky, E., 2013. Silica-sepiolite
314 nanoarchitectures. *J Nanosci Nanotechnol*. 13 (4), 2897-2907.
- 315 Grillet, Y., Cases, J., Francois, M., Rouquerol, J. & Poirier, J. 1988. Modification of the porous
316 structure and surface area of sepiolite under vacuum thermal treatment. *Clays Clay Miner.* 36, 233-
317 242.
- 318 Hadjiivanov, K., 2014. Identification and characterization of surface hydroxyl groups by infrared
319 spectroscopy. *Adv. Catal.* 57, 99-318.
- 320 Hayashi, H., Otsuka, R., Imai, N., 1969. Infrared study of sepiolite and palygorskite on heating. *Am.*
321 *Min.* 53, 1613-1624.
- 322 Ilgen, O., Akin, A.N., 2012. Determination of reaction orders for the transesterification of canola oil
323 with methanol by using KOH/MgO as a heterogeneous catalyst. *Appl. Catal. B: Envir.* 126, 342-346.
- 324 Irkeç, T., Unlu, T., 1993. An example of sepiolite formation in volcanic belts by hydrothermal
325 alteration: Kibriscik (Bolu) sepiolite occurrence. *Mineral Res. Exploration Bull.* 115, 49-68.
- 326 Kadir, S., Akbutut, A., 2003. The geology and origin of sepiolite, palygorskite and saponite in
327 Neogene lacustrine sediments of the Serinhisar-Acipayam Basin, Denizli, SW Turkey *Clays Clay*
328 *Miner.* 51, 279-292.
- 329 Kadir, S., Erkoyun, H., Eren, M., Huggett, J., Önalgil, N., 2016. Mineralogy, geochemistry, and
330 genesis of sepiolite and palygorskite in Neogene lacustrine sediments, Eski ehir Province, West
331 Central Anatolia, Turkey. *Clays and Clay Minerals* 64 (2), 1456166.
- 332 Kok, M.V., 2013. Thermal characterization of sepiolite samples *Energy Sources, Part A: Recovery,*
333 *Utilization, and Environmental Effects* 35 (2), 173-183.
- 334 Leguey, S., Ruiz de Leon, D., Ruiz, A.I., Cuevas, J., 2010. The role of biomineralization in the
335 origin of sepiolite and dolomite. *American Journal of Science* 310, 165-193.

336 Mota, C.J.A., de Lima, A.L., Ronconi, C.M., 2016. Heterogeneous basic catalysts for biodiesel
337 production. *Cata. Sci. & Technol.* 6 (9), 2877-2891.

338 Ogorodova, L.P, Vigasina, M.F., Melchakova, L.V., Kiseleva, I.A., Krupskaya, V.V., Bryzgalov,
339 I.A., 2016. Natural Mg-Fe clinochlores: enthalpies of formation and dehydroxylation derived from
340 calorimetric study. *Am. Miner.* 101(6), 1431-1437.

341 Pi kin, S., Ylmaz, M.S., Kalpaklı, Y., 2013. Thermal behavior and dehydroxylation kinetics of
342 naturally occurring sepiolite and bentonite. *J. Ther. Anal. Calor.* 114(3), 1191-1199.

343 Post, J.E., Bish, D.L., Heaney, P.J., 2007. Synchrotron powder X-ray diffraction study of the
344 structure and dehydration behavior of sepiolite. *Am. Miner.* 92 (1),91-97.

345 Post, J.L., Crawford, S.M., 2014. Uses of near-infrared spectra for the identification of clay
346 minerals. *Appl. Clay Sci.* 95,383-387.

347 Pozo, M., Calvo, J.P., Pozo, E., Moreno, Á., 2014. Genetic constraints on crystallinity, thermal
348 behaviour and surface area of sepiolite from the Cerro de los Batallones deposit (Madrid Basin,
349 Spain). *Appl. Clay Sci.* 91-92, 30-45.

350 Preisinger, A., 1959. X-ray study of the structure of sepiolite. *Clays Clay Miner.* 6, 61-67.

351 Romero, R., Muciño, G.E.G., Garcia-Orozco, I., Serrano, A.R., Jiménez, R.B., Natividad, R., 2016.
352 Deactivation study of K_2O/NaX and Na_2O/NaX catalysts for biodiesel production. *Catal. Today*,
353 271, 220-226.

354 Ruiz, J.R., Mora, M., López, M.I., Carmona, M.Á., Jiménez-Sanchidrián, C., 2010. Study of the
355 thermal decomposition of a sepiolite by mid- and near-infrared spectroscopies. *Polyhedron.* 29
356 (16),3046-3051.

357 Sabah, E., Çelik, M.S., 2005. Sepiolite: An effective bleaching adsorbent for the physical refining of
358 degummed rapeseed oil. *J. Am. Oil Chem. Soc.* 82 (12), 911-916.

359 Singer, A., 1989. Palygorskite and sepiolite. In: Dixon, J.B., Schultze, D.G. (eds): *Soil mineralogy
360 and environmental applications.* Soil Science Society of America, Madison, Wisconsin, USA, Book
361 Series 7, 555-584.

362 Soetaredjo, F.E., Ayucitra, A., Ismadji, S., Maukar, A.L., 2011. KOH/bentonite catalysts for
363 transesterification of palm oil to biodiesel. *Appl. Clay Sci.* 53 (2), 341-346.

364 Somorjai, G.A., Na, K., 2015. Hierarchically nanoporous zeolites and their heterogeneous catalysis:
365 current status and future perspectives. *Catal. Lett.* 145 (1), 193-213.

366 Suarez, M., Garcia-Rivas, J., Garcia-Romero, E., Jara, N., 2016. Mineralogical characterisation and
367 surface properties of sepiolite from Polatli (Turkey). *Appl. Clay Sci.* 131, 124-130.

368 Torres-Ruiz, J., López-Galindo, A., Gonzales-López, J.M., Delgado, A., 1994. Geochemistry of
369 Spanish sepiolite-palygorskite deposits: genetic considerations based on trace elements and isotopes.
370 *Chem. Geol.*, 112, 221-245.

- 371 Villamiel, M., Corzo, N., Foda, M.I., Montes, F., Olano, A., 2002. Lactulose formation catalysed by
372 alkaline-substituted sepiolites in milk permeate. *Food Chemistry*. 76, 7-11.
- 373 Wang, Y., Sun, G., Li, Y., Cai, Z., Teng, Y., Reaney, M.J.T., 2017. K₂CO₃-loaded hydrotalcite: A
374 promising heterogeneous solid base catalyst for biolubricant base oil production from waste cooking
375 oils *Appl. Catal. B: Environ.* 209, 118-127.
- 376 Xu, C., Liu, Q., Xin, R., Li, C., Yang, J., 2013. Application of red mud as a basic catalyst for
377 biodiesel production. *J. Envir. Sci.* 25 (4), 823-829.
- 378 Yenyol, M., 1986. Vein-like sepiolite occurrence as a replacement of magnesite in Konya, Turkey.
379 *Clays and Clay Minerals* 34, 353-356.
- 380 Yenyol, M., 2014. Characterization of two forms of sepiolite and related Mg-rich clay minerals
381 from Yenido an (Sivrihisar, Turkey). *Clay Miner.* 49 (1), 91-108.